Clim Dyn (2014) 42:1857–1872
DOI 10.1007/s00382-013-1912-8

High-resolution sea wind hindcasts over the Mediterranean area

M. Menendez · M. García-Díez · L. Fita · J. Fernández · F. J. Méndez · J. M. Gutiérrez

Received: 27 November 2012 / Accepted: 8 August 2013 / Published online: 8 September 2013

Abstract The goal of this study is to develop a high-resolution atmospheric hindcast over the Mediterranean area using the WRF-ARW model, focusing on offshore surface wind fields. In order to choose the most adequate model configuration, the study provides details on the calibration of the experimental saet-up through a sensitivity test considering the October–December 2001 period (the 2001 super-storm event in the West Mediterranean). A daily forecast outperforms the spectral technique of previous products and the boundary data from ERA-Interim reanalysis produces the most accurate estimates in terms of wind variability and hour-to-hour correspondence. According to the sensitivity test, two data sets of wind hindcast are produced: the SeaWind I (30-km horizontal resolution for a period of 60 years) and the SeaWind II (15-km horizontal resolution for 20 years). The validation of the resulting surface winds is undertaken considering two offshore observational datasets. On the one hand, hourly surface buoy stations are used to validate wind time series at specific locations; on the other hand, wind altimeter satellite observations are considered for spatial validation in the whole Mediterranean Sea. The results obtained from this validation process show a very good agreement with observations for the southern Europe region. Finally, SeaWind I and II are used to characterize offshore wind fields in the Mediterranean Sea. The statistical structure of sea surface wind is analyzed and the agreement with Weibull probability distribution is discussed. In addition, wind persistence and extreme wind speed (50 year return period) are characterized and relevant areas of wind power generation are described by estimating wind energy quantities.

Keywords Dynamical downscaling · Multiphysics · Hindcast · Offshore surface wind · WRF

1 Introduction

Ocean surface wind plays a key role in a wide variety of phenomena that have an important effect on the climate all over the world. Changes in air masses, humidity fluxes from sea surface evaporation, storm surges, or the waves, are examples of phenomena in which wind is the main driver. Offshore wind is also a key factor for many socio-economic sectors, including renewable energy and, in particular, offshore wind farms, a sector of growing technical and commercial relevance in the last decade. Wind-induced storm surge and waves are key elements in the determination of coastal risks in the Mediterranean Sea (Marcos et al. 2009). The hydrodynamic modeling of waves and sea level extreme events is highly dependent on the quality of the forcings (Weisse et al. 2012; Sanchez-Vidal et al. 2012). Therefore, a high resolution dynamic downscaling of offshore wind fields is essential for the estimation of storm oceanic events.

Consequently, in recent years there has been an increasing interest in gathering homogeneous offshore wind datasets with high spatial and temporal resolution.

M. Menendez (✉) · F. J. Méndez
Environmental Hydraulics Institute, Universidad de Cantabria, Santander, Spain
e-mail: menendezm@unican.es

M. García-Díez · L. Fita · J. Fernández
Department of Applied Mathematics and Computer Science, Universidad de Cantabria, Santander, Spain

J. M. Gutiérrez
Instituto de Física de Cantabria CSIC-UC, Santander, Spain

However, this is still a challenging problem. On the one hand, in situ observations (e.g. from ships or buoys) are spatially scarce and, thus, are only useful locally. For instance, Cavaleri et al. (1996) used surface pressure measurements from different coastal stations surrounding the narrow Adriatic Sea to produce surface wind hindcast in this area. Günter et al. (1997) used operational surface pressure analysis charts from different national meteorological institutions on the North Atlantic Sea. Meanwhile, WASA (1998) used triplets of pressure measurements to derive upper percentiles of geostrophic wind speeds in order to assess the long-term storm climate. On the other hand, satellite scatterometers are an alternative to in situ observations, though they offer short records with irregular measurements in time and space. Therefore, remote sensing data are often used to evaluate numerical hindcasts (e.g. Winterfeldt et al. 2011).

Reanalysis products are an alternative to observational data. These have been considered as quasi-observational datasets in many fields (Brands et al. 2012). Each reanalysis dataset is produced by a particular numerical atmospheric model at a global scale, providing a set of physically, spatially and temporally consistent gridded atmospheric variables for a long period of time. Examples are the popular ERA-40 and NCEP-NCAR reanalyses (with resolutions over 100 km), or the second-generation ERA-Interim or JRA-25 reanalysis (with higher resolutions, approximately 75 km). These datasets have been produced considering all the available observations at the time and, therefore, they are assumed to be an accurate representation of the atmosphere, suitable to undertake climatic studies. However, the coarse resolution of these products does not allow properly resolving regional features such as complex orography and/or coastal lines.

To obtain a detailed description of the atmosphere for regional purposes, Limited Area Models (LAMs) are run at mesoscale resolution (from 5 up to 75 km) driven by the global reanalysis, which provide the initial and boundary conditions. LAMs can be applied over domains of several 100 km^2 (Winterfeldt and Weisse 2009), and the resulting downscaled high resolution atmospheric fields can be considered proper representations of the atmospheric conditions (Giorgi 1990). Although the added value of the LAMs—compared to the global reanalysis—is still under debate for different applications, recent studies have shown that more accurate offshore wind fields are obtained applying this technique both in forecast/hindcast (Ardhuin et al. 2007) and climatic modes (Feser et al. 2011).

One of the main dynamical downscaling efforts on the Mediterranean basin, focusing on wind simulation, is described in Sotillo et al. (2005). They performed a 44-year hindcast of 50 km resolution from NCEP/NCAR global reanalysis using the REMO model (Jacob and Podzun 1997). The comparison with observations showed that the regional model improved the wind fields in the regions close to the continent as well as the extreme wind thresholds. Weisse et al. (2009) produced several datasets of atmosphere, wave and tide surges using REMO and other models, focusing on northern Europe. Winterfeldt et al. (2011) used this atmospheric dataset to show the added value of REMO with respect to the reanalysis by comparing it with satellite data from QuikSCAT. Again, the added value was concentrated in coastal areas, while REMO was slightly worse over the open oceans. These results point to the importance of optimizing the technique used to keep the regional model close to the synoptic situation that really occurred on a daily basis. Sotillo et al. (2005) and Weisse et al. (2009) used spectral nudging (von Storch et al. 2000). An equivalent result was found by Winterfeldt and Weisse (2009) using buoy data over the North Sea. In the present study, our goal is to show how the Weather Research and Forecasting (WRF, Skamarock et al. 2008) model can be used to produce high resolution wind datasets, with the advantage of being an open source, state-of-art, non-hydrostatic model that can deal with mesoscale phenomena. The study focuses on the Mediterranean Sea, which is a challenging area to model due to its complex orography, coastline, and convective weather regimes. Mesoscale phenomena play a very important role in many regions of the Mediterranean Sea, so these higher resolution simulations are expected to add value to the existing reanalysis.

This work can be summarized into three phases: (1) an analysis of the sensitivity of WRF LAM model on different configurations (Sect. 3), (2) an evaluation of the performance of the high-resolution hindcasts of offshore wind over southern Europe using instrumental measurements (Sect. 4), and (3) the characterization of the offshore wind climatologies and wind resource (Sect. 5). In the first phase, a sensitivity experiment was conducted in order to test the performance of the downscaling for the different choices and configurations, which may affect the final result (Fernández et al. 2007). Several global datasets were used as input/boundary conditions (described in Sect. 2.2), and the best physical parameterization and simulation approach-weather hindcast versus climate run (Qian et al. 2003)—were obtained. Then, special emphasis was put on evaluating the accuracy of the wind hindcast (Sect. 4) using buoy and satellite data (described in Sect. 2.1). The resulting long time series of wind were used to characterize the wind climatologies and wind energy resource (Sect. 5) in the Mediterranean region. Finally, a summary and some conclusions are provided (Sect. 6).

2 Data

2.1 Observational data

Two different sources of observed measurements have been used in the present work: buoy and satellite data. Buoys are the most commonly used instrument to collect data at sea. However, within the study domain, not many buoys are equipped with meteorological instruments, especially anemometers/wind sensors-devices. Most of the wind records are from coastal buoys which are affected by local aspects such as complex coast lines and orography. The Spanish REDEXT network is a set of offshore buoys (locations illustrated in Fig. 1) from Puertos del Estado (OPPE). These 16 buoy-stations provide wind information from an anemometer located 3 m above site elevation. The recorded period, depth and distance from the coast are described in Table 1. Wind speed and direction values have undergone a quality check (quality flags from the sensor, quality analysis from OPPE and finally our quality control to avoid outliers and jumps) and are considered a set of appropriate data. The wind speed is extrapolated from three to ten meter heights using the wind profile power law with an exponential coefficient of 0.11 (Hsu et al. 1994).

Although in situ observations are considered the most reliable, most records are not longer than 10 years, they have important gaps and are scattered in space. In contrast, satellite wind measurements provide the best possible spatial coverage to evaluate the Mediterranean region. We use the wind speed values at a height of 10 meters derived from the backscatter coefficient of altimeter measurements. The ascending and descending data from five missions: Geosat, Topex/Poseidon, Jason-1, Envisat and Geosat Follow-On (GFO) are assembled. The time resolution of the satellite data depends on the mission, with a minimum time lapse of 9.9 days for Topex and Jason, to 30–35 days for Envisat. The measurements are taken between the years 1986 and 2008. Wind data from each satellite mission are combined in a dataset of 4.110.309 values to compare them with simulation outcomes. Although satellite tracks exclude any possibility of deriving hourly time series at a location, they provide good spatial coverage (Fig. 1) to evaluate the dynamical downscaling over the whole Mediterranean region. This satellite dataset has been used for the sensitivity analysis on model configuration (Sect. 3.2) and for the validation process (Sect. 4).

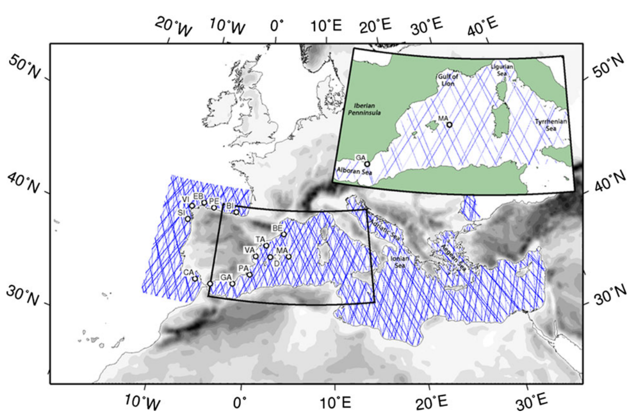

Fig. 1 Model simulation domain and orography (*grey shades*). Satellite tracks and buoy locations used in the validation are also shown. The *inset* shows the subset of observational data (satellite tracks and buoys) used in the sensitivity tests (October through December, 2001)

2.2 Global reanalysis data

Reanalyses are datasets devoted to reproduce past atmospheric fields as accurately as possible. To achieve this, state-of-the-art models are used in retrospective form to assimilate all quality-controlled observations available over long periods of time, providing plausible states of the atmosphere, compatible with observations. The model version is frozen and, therefore, reanalyses do not suffer from the inhomogeneities caused by operational model updates, and have been successfully used in a large number of meteorological and climatic studies (see Brands et al. 2012).

In this work, some of the most popular global reanalyses have been used: ERA-40 (Uppala et al. 2005) from the European Centre for Medium Range Weather Forecasts (ECMWF), NCEP/NCAR Reanalysis (Kalnay et al. 1996) from the National Center for Environmental Prediction (NCEP) and the National Center for Atmospheric Research (NCAR), and ERA-Interim reanalysis (Dee et al. 2011). Table 2 summarizes their main characteristics. All these reanalysis are widely used in different applications: ERA-40 and ERA-Interim have higher spatial resolution, whereas NCEP/NCAR reanalysis cover a longer period. In ERA-interim, several biases found in ERA-40 were corrected, offering a higher resolution and a more advanced assimilation process, but covering a significantly shorter period of time. Reanalysis going back from 1979/1989 do suffer from inhomogeneities due to the introduction of satellite data (Bengtsson et al. 2004). Thus, choosing the appropriate reanalysis dataset for a given application is not a simple task, and this motivates their inclusion in the sensitivity tests described in Sect. 3.

3 Numerical wind simulation

3.1 Experimental setup

The Weather Research and Forecasting (WRF) model with the Advanced Research dynamical solver (WRF-ARW)

Table 1 Main characteristics of buoys used in model comparison

Station (code)	Location (°)	Depth (m)	Dist. from shore (km)	Collection period
Cabo Begur (BE)	41.92N, 3.66E	1,200	24	2002-present
Bilbao-Vizcaya (BI)	43.64N, 3.05W	600	18	2002-present
Cabo de Gata (GA)	36.57N, 2,34W	536	30	1998-present
Cabo de Palos (PA)	37.65N, 0.33E	230	30.5	2006-present
Golfo de Cadiz(CA)	36.48N, 6,97W	450	40.5	1996-present
Dragonera (DR)	39.56N, 2.1E	135	54	2006-present
Estaca de Bares (ES)	44.16N, 7.62W	1,800	21	1998-present
Mahon (MA)	39.72N, 4.44E	300	21.5	2004-present
Cabo de Peñas (PE)	43.74N, 6.17W	615	31.5	1998-present
Cabo Silleiro (SI)	42.13N, 9.39W	600	39	1998-present
Tarragona (TA)	40.68N, 1.47E	688	50.5	2004-present
Valencia II (VA)	39.52N, 0.21E	260	36	2005-present
Villano-Sisargas (VI)	43.5N, 9.21W	386	15.5	2001-present

Table 2 Main characteristics of the reanalysis datasets that have been used in the present study

Global reanalysis	Period (years)	Resolution (spectral)	Approx. resolution (°)
ERA40	1957.9–2002.8	T159	1.125
NCEP/NCAR	1948-present	T62	1.875
ERA-Interim	1989-present	T255	0.703

(Skamarock et al. 2008) is an open source atmospheric model widely used by the scientific community. In the present work, WRF-ARW version 3.1.1 has been used, which was released in April 2009. It has a non-hydrostatic core, grid- and spectral-nudging capabilities and it provides a large number of different options to parameterize key sub-grid scale physical processes. A modification of the WRF model code, known as CLWRF (Fita et al. 2010), was used to retrieve the mean hourly wind out of the model time-step instantaneous values.

The domain of integration is a large region that encompasses the entire Mediterranean basin and a large portion of the European continent (see Fig. 1). A Lambert conformal conic projection is applied to the grid domain in order to obtain a minimum distortion in the Mediterranean grid-cell size. The model resolution is defined with 40 vertical hybrid levels (7 first levels below the first 1,000 m) and 15-km horizontal resolution (390 × 250 grid points). A sponge zone of 10 grid points relaxes the solution in the interior of the domain towards the reanalysis data on the boundaries. This resolution has been used in the sensitivity analysis (Sect. 4) and in the high-resolution 20-year hindcast (Sect. 5). A medium-resolution (30 km) with a similar setup was used to generate a 60-year hindcast product (Sect. 5).

Table 3 WRF configurations that have been tested for the period October–December 2001

Label	Running mode	PBL	Reanalysis
E1	Reforecast	YSU	ERA-40
E2	Reforecast	MYJ	ERA-40
E3	Reforecast	ACM2	ERA-40
I1	Reforecast	YSU	ERA-INTERIM
I2	Reforecast	MYJ	ERA-INTERIM
I3	Reforecast	ACM2	ERA-INTERIM
N1	Reforecast	YSU	NCEP
N2	Reforecast	MYJ	NCEP
N3	Reforecast	ACM2	NCEP
N4	Climatic (grid nudging)	YSU	NCEP
N5	Climatic (spectral nudging)	YSU	NCEP
N6	Climatic (no nudging)	YSU	NCEP

A wide spectrum of issues must be taken into account when choosing the model configuration for the production of a large dataset, such as the present high resolution wind hindcast. The choices of the physical parameterizations, the running mode (see below) and the global reanalysis used as initial and boundary conditions are not straightforward. Different studies (e.g. Günter et al. 1997; von Storch et al. 2000; Weisse and Feser 2003; Castro et al. 2005; Lo et al. 2008; Rockel et al. 2008) have analyzed a variety of model configurations but literature dealing with offshore winds is scarce. Thus, in this study, we evaluate twelve different model configurations during the October–December 2001 period, which includes a super storm, in an attempt to find the most suitable one for dynamical downscaling of offshore winds. The suitability depends on the goal pursued in the final product, which in our case is the ability to represent realistic day-to-day wind variability. The configurations

Table 4 Main characteristics of the physical parametrizations that have been used with WRF

Parametrization scheme	Code	Scheme name	Main characteristics	References
Surface layer	1	MM5	Similarity model based on Monin–Obukhov and Carlson-Boland	Hong et al. (2006)
	2	Eta	Similarity via look-up tables Monin–Obukhov with Zilitinkevich, thermal roughness length	Janjić (1990, 1994)
	7	Pleim-Xiu	Similarity theory, parametrization of a viscous sub-layer, accounts of differences in the diffusivity of heat, water vapour, and trace chemical species, similarity functions estimated from state variables	Pleim (2006)
Boundary layer	1	YSU	Non local scheme, buoyancy dependence, entrainment scheme. (Improvement of previous MM5 MRF scheme)	Hong et al. (2006)
	2	MYJ	2.5 level local scheme. TKE computation (BL in Eta model)	Janjić (1990, 1994, 2002)
	7	ACM2	Non local transilient scheme in unstable conditions that turns to local in stable conditions	Pleim (2007a, b)
Land surface	2	Noah	Soil temperature and moisture in four layers, fraction of snow and ice	Chen and Dudhia (2001)
Microphysics	4	WRF S-M 5	Single-Moment scheme with, vapor, rain, snow, cloud ice, and cloud water	Hong and Lim (2006)
Cumulus	3	Grell-Devenyi	Average of an multi-parameter ensemble for each gridpoint	Grell and Devenyi (2002)
Long wave radiation	3	RTTM	Spectral-band scheme using the correlated-k method	Mlawer et al. (1997)
Short wave radiation	3	Dudhia	Downward integration of short wave flux, with clear-air scattering, water vapor absorption and cloud albedo and absorption	Dudhia (1989)

Note that each boundary layer scheme is paired with a surface layer scheme

tested are defined in Table 3 and encompass three of the most popular planetary boundary layer schemes (PBL), three reanalysis datasets, and four running modes. The PBL schemes are described in Table 4 (a detailed description in García-Díez et al. 2012), the global reanalyses are described in Sect. 2.2 and Table 2, and the four running modes are described next.

3.1.1 *Continuous run, no nudging*

The integration was carried out in a single continuous simulation. No nudging was applied. This simulation began on September 1st, 2001, leaving one month as spin-up.

3.1.2 *Continuous run, grid nudging*

The integration was carried out in a single continuous simulation. Grid analysis nudging was applied above the PBL at every time step. In grid nudging, the 3D grid-points of the model are nudged using Newtonian relaxation (Charney et al. 1969) to a grid 4-dimensionally interpolated from the analysis (Stauffer and Seaman 1990). This simulation also began on September 1st. The nudged variables were zonal and meridional winds, temperature, and specific humidity.

3.1.3 *Continuous run, spectral nudging*

The integration was carried out in a single continuous simulation. Spectral nudging of the largest scales was applied at every time step. This simulation also began on September 1st. Spectral nudging is a technique to drive the large scale (long wave) in LAM model simulations (von Storch et al. 2000), so it stays close to the large scale of the driver coarser resolution model. Short wave variability and low level evolution of the atmosphere are allowed to be freely produced by the LAM dynamics. The nudged variables were wind components, temperature, specific humidity and geopotential. The top wavenumbers nudged in each direction were 3 for x and 2 for y. The nudging was not applied to the lower 10 model levels.

3.1.4 *Re-forecast run (RF)*

As the atmosphere is highly non-linear, short wave variability does interact with long wave, and nudging techniques do not allow for these interactions to fully develop. The so-called reforecast running mode does not suffer from this problem, as it performs short simulations and concatenates them to build a quasi-continuous dataset (Lenderink et al. 2009; Hu et al. 2010; Jiménez and Dudhia 2012). In this study, daily simulations were started from reanalysis data at 6 UTC every 24 h and were run for 42 h. A sensitivity test, varying the overlap time at hourly steps, was carried out to optimize the time of day for the overlap of the simulations. Statistics were computed in order to know at which time the differences were minimum between a pair of overlapping simulations. This analysis concluded that the best time was 18 UTC, thus 12 h are dropped as spin-up.

3.2 Sensitivity analysis

The Mediterranean Sea is one of the most cyclogenic regions in the northern hemisphere during winter, when episodes of extreme weather are common. The highest frequency of wind storms occurs in its northwestern basin (Lionello et al. 2006a, b), and is associated with E-NE and NW intense atmospheric fluxes. Model performance is analyzed in the western Mediterranean basin for a period covering 3 months, from October to December 2001. This period is chosen since it contains one of the most extreme cyclogenetic events recorded in the Western Mediterranean (Arreola et al. 2003; Genovés and Jansà 2003; Fita et al. 2007). This particular event formed in November 2001, when a strong blocking pattern developed over the eastern Atlantic and pushed a polar air mass over the Iberian Peninsula, unusually cold for the season. The cold air reached the warm Mediterranean Sea, leading to a complex cyclogenesis with contributions from dynamical, diabatic and orographic forcings. In spite of this particularly strong event, a three-month period such as this one is assumed to be large enough to ensure a wide spectrum of atmospheric situations. In addition, this period presents wind records from buoys and satellite data for comparison with results simulated by WRF. The subplot of Fig. 1 shows the validation region for the sensitivity tests and observational data for this period.

In the present section, the main results of the sensitivity tests are explained. Note that the 12 WRF configurations (see the labels in Table 3) produce a set of 12 realizations of the meteorological evolution during the period between October and December 2001 in this area. This information can be easily summarized by using a Taylor diagram (Taylor 2001) since it is particularly useful in assessing the relative merits of competing models. The associated value of the 12 realizations to each value of the satellite data was determined for the analyzed period. As the observed altimeter measurements are not regularly spaced, the associated values of the realizations are the closest model grid-point in space and time. On a Taylor diagram, the correlation coefficient and the centered root-mean-square deviation (RMSD) of the estimated pairs of data between altimeter observations (y) and model simulations (x) are all indicated by a single point on a two-dimensional graph (Fig. 2).

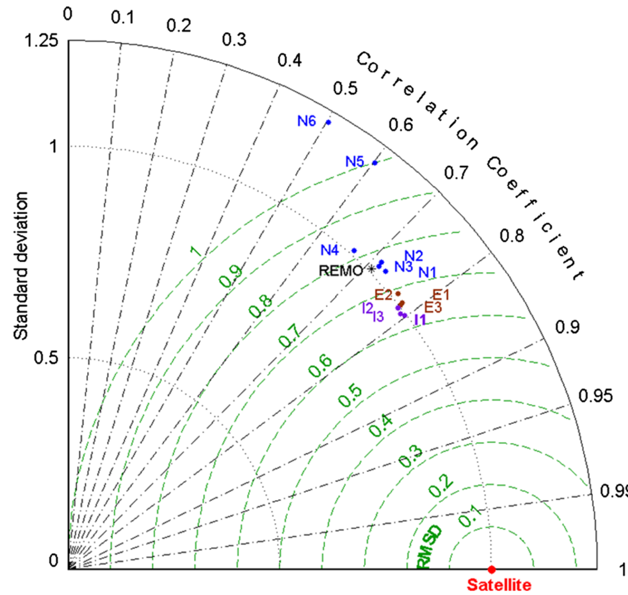

Fig. 2 Taylor diagram displaying statistical comparisons of the 12 analyzed realizations (see on Table 3 the description of labels) and the REMO hindcast estimated with satellite observations as reference, for October–December 2001

$$RMSD = \sqrt{\frac{1}{N}\sum_{i=1}^{N}\left[(y_i - \bar{y}) - (x_i - \bar{x})\right]^2} \tag{1}$$

Note that these data pairs along satellite tracks combine the space and time dimensions and, therefore, the correlation is both spatial and temporal. All the selected values from the realizations are, in the last step, re-scaled with the standard deviation of the satellite observations, so the reference point of the satellite data is located at one standard deviation. A comparison with other downscaling output from HIPOCAS project (Sotillo et al. 2005) is also shown, labeled REMO. The Taylor diagram compares the performance of all the configuration variants. A colour is assigned to the experiments from similar reanalyses.

Realizations using ERA-Interim reanalysis present the best performance, confirming this reanalysis as the most accurate. The best among the 12 realizations is the one using the YSU PBL scheme, reforecast running mode and ERA-INTERIM boundary conditions (I1), with a correlation of $\sim$0.8 and an RMSD lower than 0.65; however, I2 and I3 also show a good performance. The realizations corresponding to ERA-40 exhibit a good performance although RMSD are closer to 0.7 and, finally, the ones using NCEP form a separate group, showing lower correlation values ($\sim$0.72) and RMSD above 0.75. The NCEP-nested realizations are close to REMO, which was also forced by NCEP.

Regarding the running mode, the reforecast mode realizations show a smaller RMSD and larger correlation than the continuous ones. As expected, the run with no nudging (N6) shows the worst performance of all, with a modest correlation of 0.5 and a large root mean square error. The run using grid nudging (N5) improves the correlation of N6 by 0.1, but does not improve the standard deviation, which still suffers from a similar overestimation of approximately 25 %. In contrast, the run using spectral nudging (N4) solves this problem, and shows a standard deviation very similar to the observed one, close to Sotillo et al. (2005). The causes of this behavior are unclear. To address them, maps of mean wind and standard deviation were plotted (not shown). The analysis reveals that the difference in the standard deviation is related to more intense average winds in some regions. In the run with no nudging (N6) these areas tend to appear close to the eastern boundary of the domain. As the westerlies are the dominant flow, this points to consistency problems in the outflow of the wind along the eastern boundary. The authors conclude that the reforecast running mode is the one showing the best skill. Other studies (Lo et al. 2008) found the run using spectral nudging to be more skillful than the reforecast run, but in those cases had used a significantly larger restart period (1 week). This work shows that frequent restarts (i.e. 24 h) can improve the skill obtained using spectral nudging despite the spin-up problems. In general, the model skill shows a small sensitivity to the PBL parametrization schemes, however, realizations using the YSU scheme are slightly better that the others for the three reanalyses.

According to the previous results, WRF run in re-forecast mode, nested into ERA-Interim Reanalysis and using the YSU PBL scheme provides the most accurate representation of past surface wind. However, ERA-Interim is available for a short period of time, not appropriate to estimate extreme regimes or decadal variability. Therefore, we produced two different products within the framework of this project. First, in order to have a long wind hindcast spanning from 1950 suited for climate studies, NCEP/NCAR re-analysis was used to produce a lower resolution (30-km) wind hindcast, hereafter referred to as SeaWind I. Then, ERA-Interim was used as global re-analysis for the high-resolution wind hindcast production (15-km) from 1989 over the same domain (hereafter SeaWind II). In both products, the running mode was reforecast and the PBL parameterization scheme was the non-local closure YSU scheme.

4 Performance of SeaWind hindcasts

An exhaustive validation of the surface wind hindcast products, SeaWind I and SeaWind II, against observations (buoy and satellite data) has been accomplished. Several diagnostic statistics (Bias, scatter index (SI), root mean square (RMS) error and Pearson correlation) have been calculated to evaluate the model performance with respect to instrumental data (x SeaWind values and y observations).

$$BIAS = \sum_{i=1}^{N} \frac{(x_i - y_i)}{N} \tag{2}$$

where N is the sample size. Bias provides the systematic difference between model and observed data.

$$SI = RMS/\bar{x}, \tag{3}$$

which measures dispersion with respect to the line $x = y$, and RMS error means the root mean square error.

$$RMS = \sqrt{\frac{1}{N}\sum_{i=1}^{N} (x_i - y_i)^2} \tag{4}$$

The Pearson's correlation coefficient (ρ):

$$\rho = \frac{\mathrm{cov(x, y)}}{\sigma_x \cdot \sigma_y}, \tag{5}$$

where $\mathrm{cov}(x,y)$ represents the covariance between two variables and σ is the standard deviation.

The pairs from observations-SeaWind hindcast were selected by taking the nearest grid point of the model and temporally interpolating the simulated data to the buoy location. Figure 3 shows a diagnosis of the comparison between the wind records from the SeaWind hindcast and three buoys in the Atlantic Ocean next to the Gibraltar Straight, North and South of the Western Mediterranean basin, respectively. The differences between the observed and modeled mean and standard deviation are negligible. The quantiles of the qq-plots have been estimated on a Gumbel scale, which allows a more detailed representation of the maximum values. This comparison shows how both SeaWind I and SeaWind II present almost identical quantile distributions that fit the observations very well, even for extremes. The biases obtained are low, with slightly lower values for SeaWind I than SeaWind II. SeaWind II presents lower SI values and higher correlation than SeaWind I, indicating a reduction of spread between observed and modeled data pairs and higher temporal correspondence.

Figure 4 shows Pearson correlation coefficient, Bias and RMS error maps for hindcasts of SeaWind I and II versus observations from all the analyzed buoys and altimeters. Due to the scattered distribution of buoy locations, the only way to validate numerical outcomes over the whole domain is by comparing them with satellite observations. Satellite-SeaWind hindcast comparison was performed by (1) selecting the corresponding simulated value for each satellite observation observations and (2) aggregating the pairs of data to

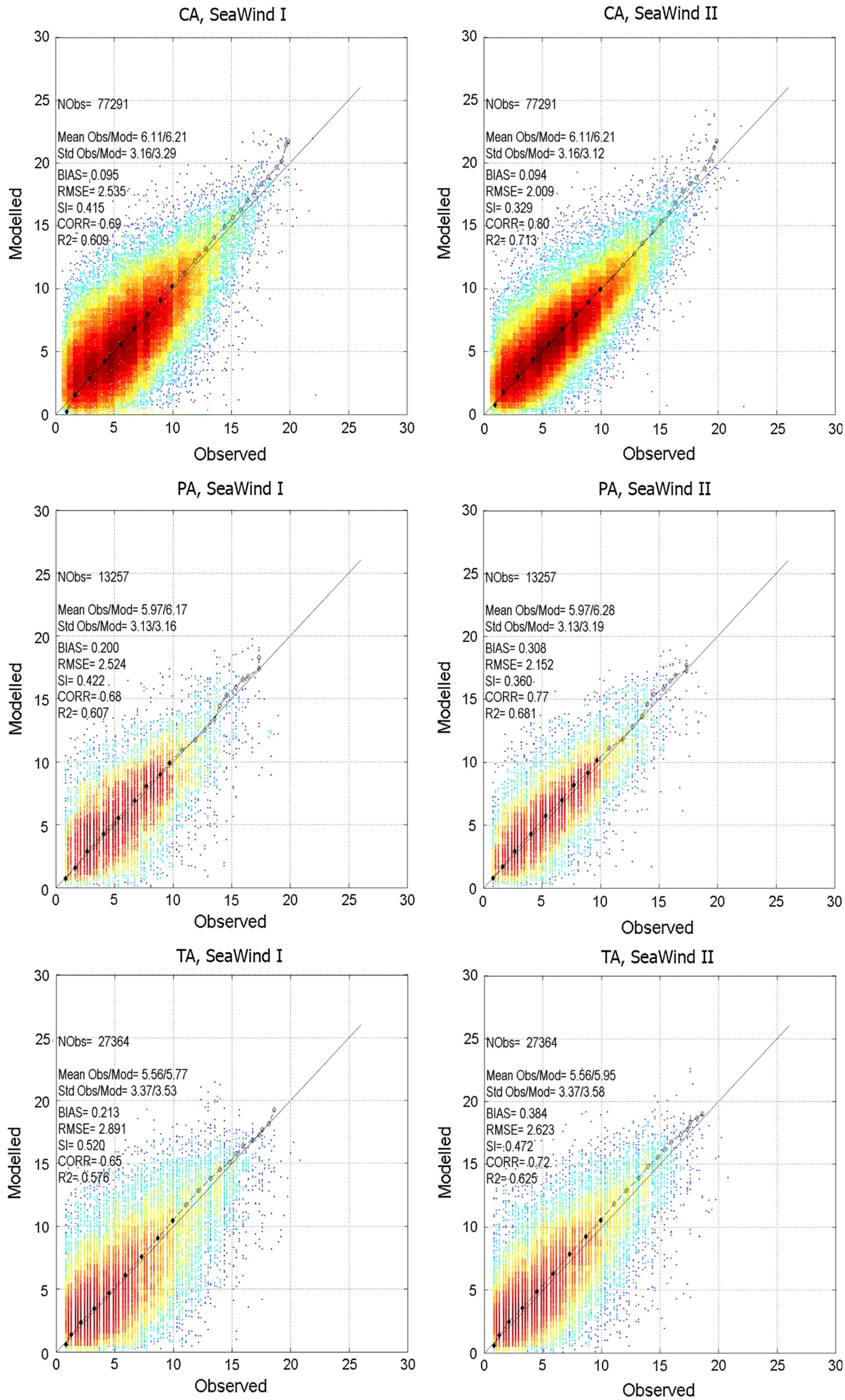

Fig. 3 Scatter diagrams, qq-plots and several statistical indices of the buoy measurements (*x-axis*) and the WRF model results (*y-axis*). *Diamonds* represent the quantile values in equally spaced Gumbel scale. *Coloured dots* are the data pairs of wind speed (m/s), which *colour intensity* represents the density of data. The name, location and others properties of the buoys are described in Table 1

grid boxes of 1 × 1°, seeking a compromise between a representative number of data per cell and the highest spatial resolution. Despite the difference in time period and time resolution between buoys and altimeters, and the local effects in buoys stations not considered on the 1 × 1° satellite boxes, the spatial distribution of the statistical

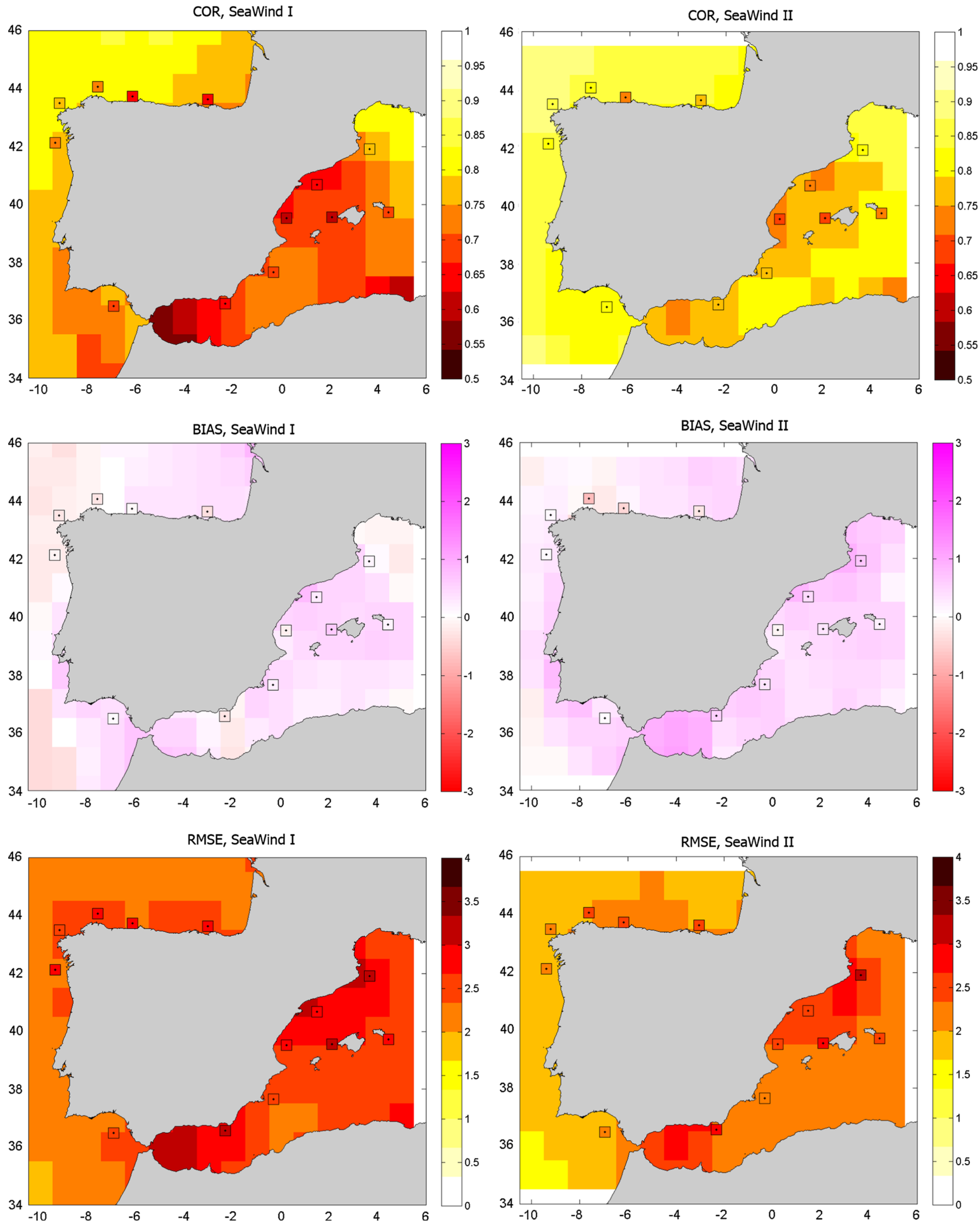

Fig. 4 Spatial distribution of the correlation, BIAS and RMSE coefficients for the intercomparison between the reanalyses and offshore stations (*squares*) or reanalyses and satellite measurements (*surface maps*)

indices shows a similar pattern (Fig. 4), reinforcing the use of satellite wind speed observations for meaningful comparisons. A positive bias in SeaWind I, lower than 1 m/s, can be inferred, whilst SeaWind II shows an even lower positive bias in the Mediterranean Sea and a minor negative bias in the open Atlantic region. Correlation and RSME estimations indicate SeaWind II agrees better with observed wind speed than SeaWind I. The main discrepancy between the SeaWind hindcasts and observations is found in the Strait of Gibraltar and the small basin between the Balearic Islands and the Iberian coast. This lower correlation and higher RMSE can be attributed to the complex topography of the nearby land

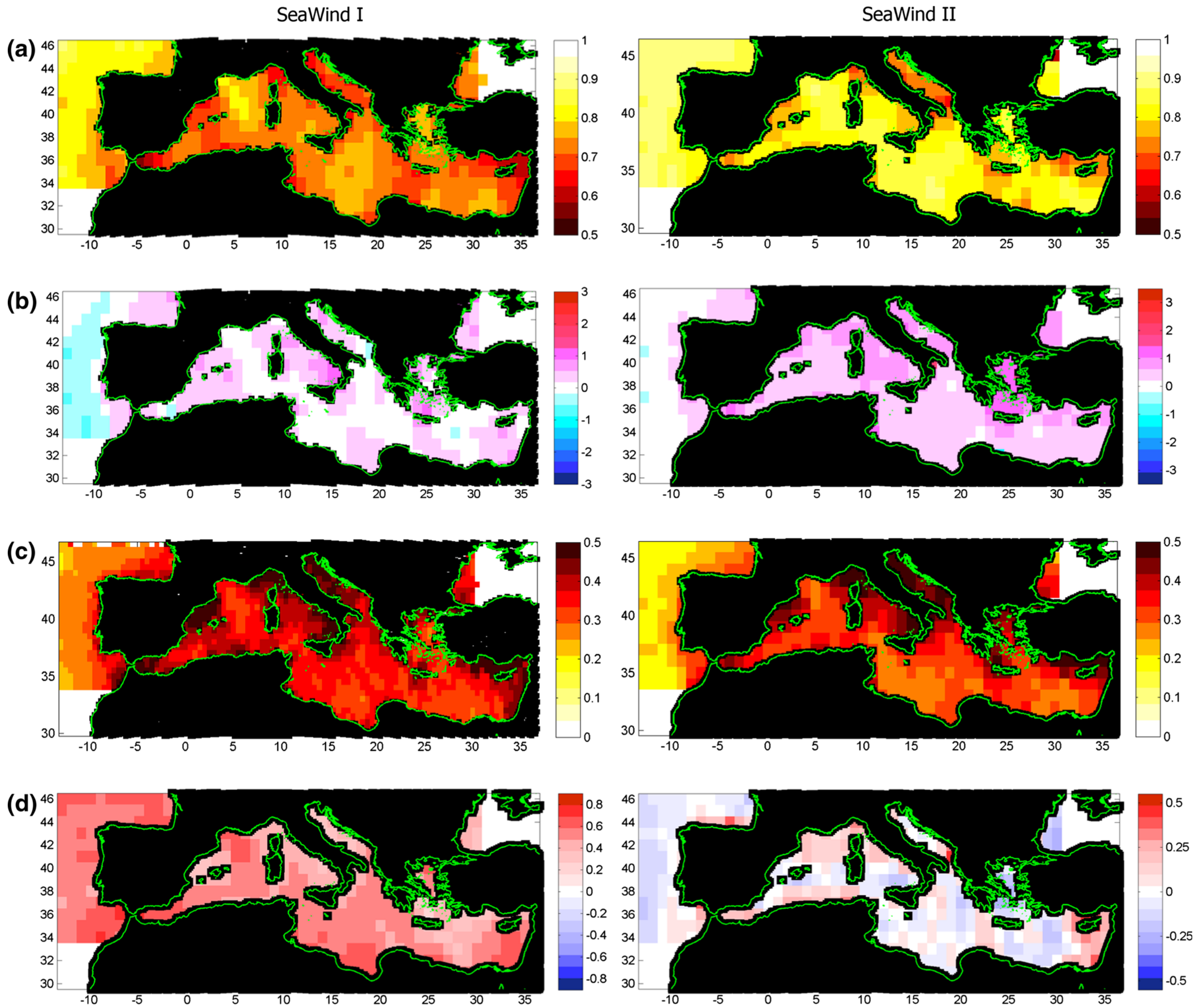

Fig. 5 Wind speed comparison of reanalysis SeaWind I and SeaWind II against altimeter observations for the 1986–2008 period. Temporal correlations (**a**), bias (**b**), Scatter index (**c**) and Brier skill score (**d**). Brier skill score is analyzed for the 1989–2008 period

areas and local factors linked to them. SeaWind II hindcast provides a better fit in these regions due to its higher spatial resolution and quality of the boundary data. The quality of SeaWind I and II hindcasts has been evaluated against satellite observations over the whole Mediterranean Sea (Fig. 5). For practically all the modelled offshore wind fields, correlation is above 0.8 and the Scatter index below 0.35 for SeaWind II (0.75 and 0.375 respectively for SeaWind I), whilst the bias does not usually reach 0.25 m/s. Despite the improved correlation, the bias is larger in SeaWind II than in SeaWind I by some tenths of m/s. The reason behind this increase is unclear, as it could be related to the different resolution or to the different initial conditions. The best results are found in the Ionian Sea, and a particularly realistic wind speed is provided in the Aegean Sea. The complicated morphology of the Mediterranean sub-basins, with many gulfs and islands and sharp orographic features, produces a relatively worse correlation coefficient and scatter index in the eastern part of the Strait of Gibraltar, Ligurian Sea, gulf of Venice and the sea between Sicily and Tunisia.

The added value of SeaWind I and SeaWind II dynamic downscaling in comparison with the driving reanalyses (NCEP and ERA-Interim, respectively) is investigated by estimating the Brier skill score test as Winterfeldt et al. (2011). The Brier skill score (BSS) used here is given by:

$$BSS = \begin{cases} 1 - \left(\sigma_D^2 \sigma_R^2\right), & \sigma_D^2 \leq \sigma_R^2 \\ \left(\sigma_R^2 \sigma_D^2\right) - 1, & \sigma_D^2 > \sigma_R^2 \end{cases} \tag{6}$$

where σ_D^2 represents the error variance of the downscaling (SeaWind) and σ_R^2 represents the error variance of the reanalysis. The satellite dataset serves as an estimate of real wind speed in the error variance assessment. BSS can vary between −1 and +1. Negative values indicate a better performance of the reanalysis and positive values an added value of the regionally modelled winds (SeaWind). The added value assessment is carried out for the years 1989–2008. BSS may introduce uncertainties due to the different temporal and spatial resolution of satellite, SeaWind I and II, and ERA-Interim and NCEP reanalyses. However, this is partly inevitable to find out whether SeaWind is able to add value to the coarser reanalysis by means of comparing it with a high resolution dataset (satellite observations).

Results of the BSS from Eq. (5) are displayed in Fig. 5d. The positive BSS values of SeaWind I indicate the added value of the downscaling procedure since NCEP reanalysis has a coarse spatial resolution of almost 2 degrees and 6 hourly values. Higher BSS values are located on the north coast of Spain, Atlantic and Mediterranean regions near Gibraltar Straight, Gulf of Lion, Libyan offshore coast, Ionian Sea and south-eastern Mediterranean basin. SeaWind II is unable to add value on the open Atlantic ocean. However, positive values are found in north coast of Spain, Gibraltar Straight, Gulf of Lion, Algerian coast, Ligurian Sea and eastern Mediterranean Sea. These regions are characterized by marine winds from onshore and mesoscale phenomena with winds modified by the orography. At high wind speeds, SeaWind II adds value over the whole Mediterranean basin (map not shown).

5 Offshore SeaWind analysis

The evaluation undertaken in the previous section confirms that SeaWind I and II hindcasts are a reasonable representation of historical surface wind fields over the Mediterranean Sea. Therefore, in this section we use these datasets to show the simulated high-resolution Mediterranean surface wind climatology, the adequacy of the Weibull distribution to the Mediterranean winds and derived products with multiple applications, such us the evaluation of wind energy resource, navigation and logistic activities, or offshore engineering design, as examples of the potential of the new databases.

5.1 Offshore wind climatology

Figure 6 shows the seasonal wind speed climatologies for ERA-INTERIM and SeaWind II, together with their land

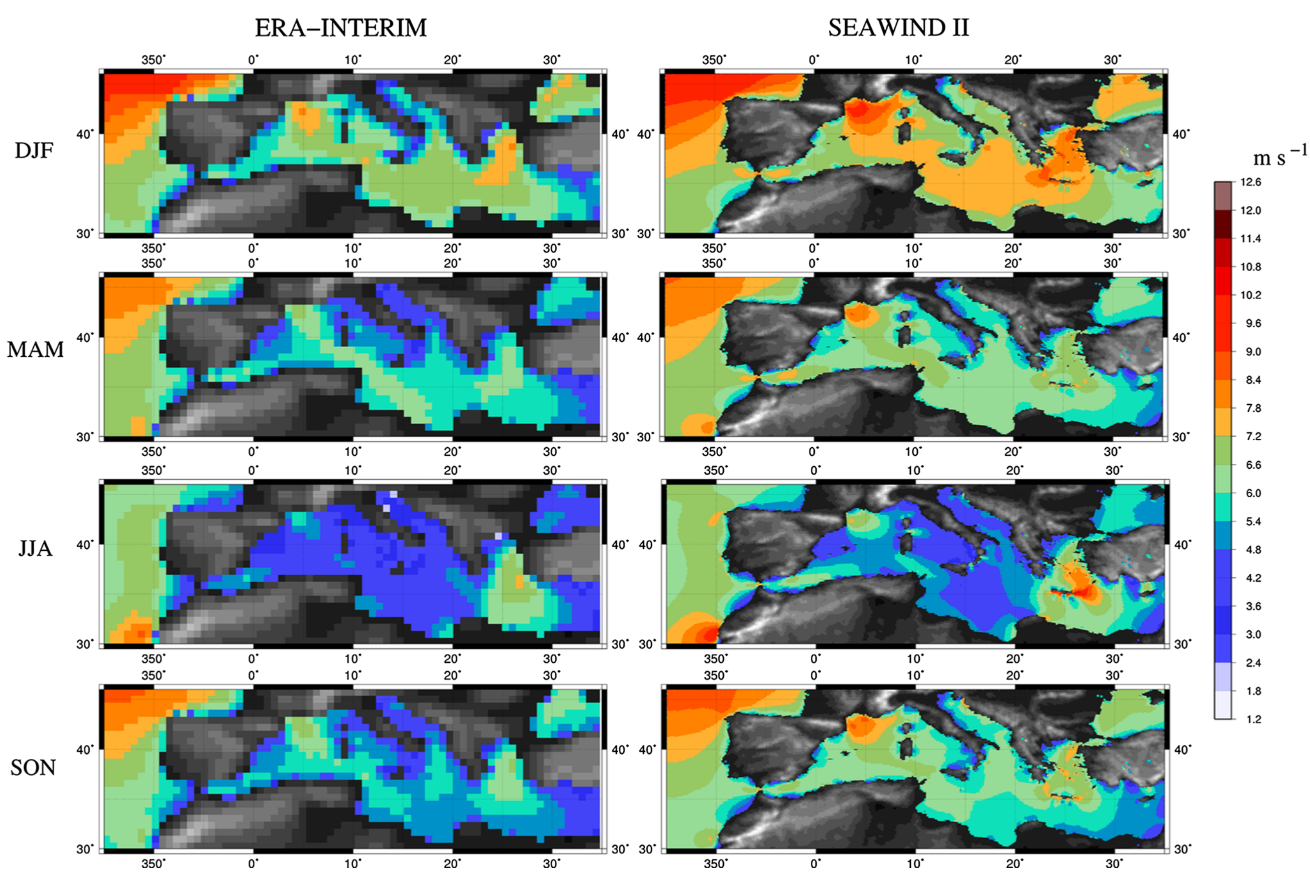

Fig. 6 Seasonal mean wind speed for ERA-INTERIM at 0.7° resolution (*left*) and SeaWind II (*right*). The base period is 1989–2009

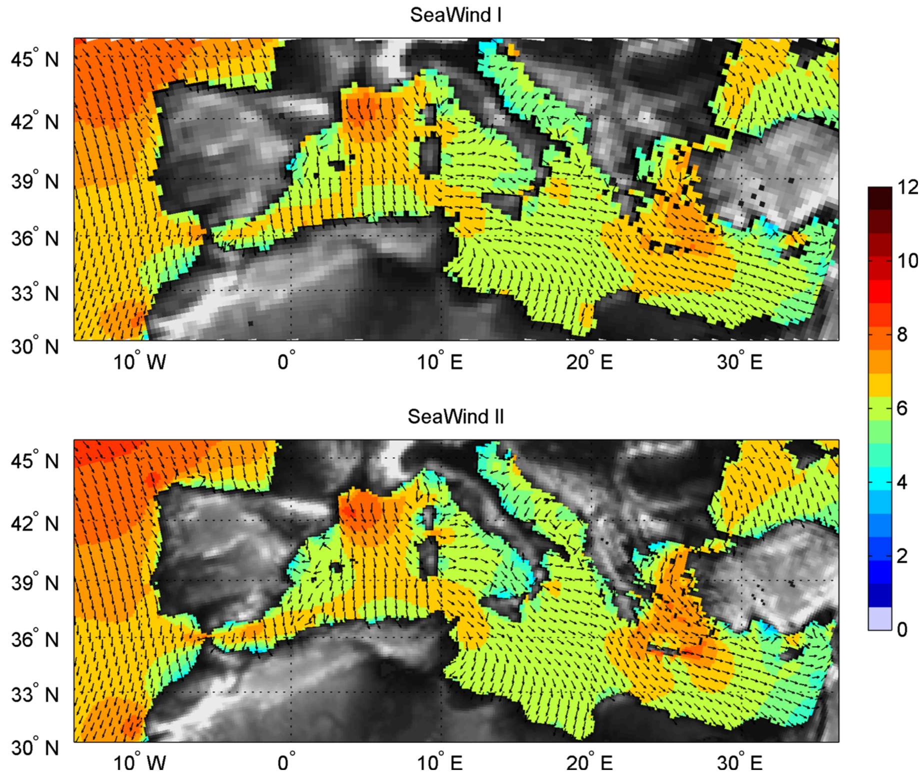

Fig. 7 Map of the mean annual offshore wind fields (m/s) of the SeaWind I and SeaWind II reanalysis

masks and topography. The main benefit of high spatial resolution of SeaWind II downscaling is the ability to represent atmospheric processes in more detail. SeaWind II is able to simulate the effect of orography over the offshore areas close to the coast more accurately and provides higher wind speed during winter season for the whole Mediterranean Sea. The high-resolution hindcast is able to model strong winds during other seasons in the cyclogenetic regions (for example, the Gulf of Lion during autumn and spring or the Meltem wind during summer in Crete). Also the wind maxima associated to the straits can be clearly distinguished in the SeaWind II climatology (straits of Gibraltar, Boniface, Messina, etc.), and not in the global reanalysis. The seasonal patterns described by SeaWind II agree with the seasonal means obtained from QuickSCAT satellite observations by Chronis et al. (2011). Moreover, SeaWind II is able to reproduce seasonal variability over coastal areas with high winds (e.g. Aegean sea) which cannot be estimated from satellite data.

Figure 7 shows the estimated mean surface wind speed for SeaWind I and II hindcasts. Northern winds (e.g. Tramontane or Mistral) dominate the western Mediterranean basin and drive severe winds over the Gulf of Lion. They are caused by a high-pressure area in the NW Europe and the acceleration of the flow when passing between the Pyrenees and the Alps. Apart from the Gulf of Lion in the western Mediterranean basin, mean wind speeds higher than 7 m/s can be found in the Gibraltar Strait and the strait between Sardinia and Corsica, which are relevant from a navigational point of view. The etesian winds are the prevailing winds blowing from northern or north-western directions over the Aegean Sea. They result from a larger circulation system over the whole eastern Mediterranean. Etesian wind is produced by the combination of high pressure over the Balkan Peninsula and low pressure over Turkey, generally of thermal origin. Note that mean annual winds over 7 m/s (orange surfaces in Fig. 7) can be considered potential areas for offshore wind energy extraction and coarser resolution hindcasts are unable to capture these realistic mean wind intensities (see for example Fig. 6).

5.2 Adequacy of Weibull distribution

Historically, the Weibull distribution has generally been accepted to represent the statistical structure of the surface wind speed probability density function (PDF), particularly over water surfaces (e.g. Pavia and O'Brien 1986; Monahan 2006). Moreover, Weibull distribution is increasingly used in the offshore wind industry. Wind speed (W) is considered a random variable following a two-parameter Weibull PDF,

$$f(W; c, k) = \frac{k}{c}\left(\frac{W}{c}\right)^{k-1} \exp\left[-\left(\frac{W}{c}\right)^{k}\right], \tag{7}$$

where c is the scale parameter and k the dimensionless shape parameter. The exponential, Gaussian and Rayleigh

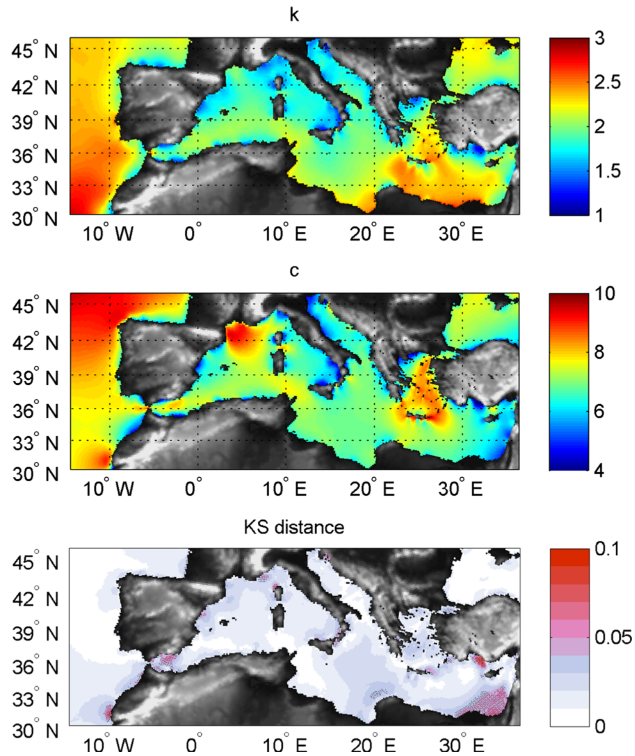

Fig. 8 Maps of the estimated scale (**c**) and shape (**k**) Weibull parameters and KS goodness of fit test for SeaWind II. *Dotted areas* show not significant grid-points at 0.01 significance level

distributions are special cases of combinations of these parameters. A number of Weibull fitting methods exist (Pryor et al. 2004), with negligible differences on estimators for large sample sizes, so, in this paper the moments method is used to fit the Weibull distribution.

Upper panels in Fig. 8 display the Weibull shape and scale parameter fields estimated from the SeaWind dataset. The spatial structure of the scale parameter c is essentially identical to that of the mean wind speed. The Weibull shape parameter k is generally close to 2 in the Mediterranean, with lower values in protected coastal areas and higher values, between 2 and 3, over the south-eastern basin (throughout the Egyptian coast and Aegean Sea). Larger values of the shape parameter are due to the occurrence of unusual events, either because of the presence of local extremes or because of steady winds of weak variability. The association of the Weibull parameters with the wind field characteristics was noted previously in Pavia and O'Brien (1986) and Monahan (2006) for other regions.

Despite the reasonable accuracy of the Weibull approximation on a global scale, deviations from the observed sea surface wind speed PDFs and the Weibull structure have been noted for some regions. For example, surface wind in the tropics does not follow Weibull behaviour (Erickson and Taylor 1989; Bauer 1996; Monahan 2006). We have evaluated the Weibull behaviour over the southern Europe sea wind speed using the Kolmogorov–Smirnov (KS) test. The KS test is a non-parametric statistical criterion that compares CDFs directly, making it unnecessary to group the wind observations into arbitrary categories and consequently, it is more sensitive than other tests to deviations in the tails of distribution. The KS-distance (the greatest difference between the empirical CDF and the fitted Weibull distribution) is shown in the bottom panel of Fig. 8. The grid-points not passing the test of 0.01 significance levels are dotted. Most of the analyzed domain shows negligible KS distances, although some small areas close to the coast (NW Alboran Sea, northern Corsica, the coast of Turkey in northern Cyprus, and southeast of the Mediterranean Sea) reveal statistical deviations from Weibull structure. The deviations from Weibull can be due to: (1) a different behaviour in the empirical relationship between the skew and the ratio mean/standard deviation of the wind speed and (2) a non-stationary wind CDF (at seasonal or interannual time-scales), causing time-dependent Weibull parameters.

5.3 Offshore wind energy potential, wind persistence and extreme winds

Successful capability of offshore wind energy generation relies on accurate estimation of wind power properties at sea. The CDF of the wind speed dictates, to some extent, the wind power distribution. The available wind power per unit area, E, is proportional to the wind speed (W) cubed and can be calculated as.

$$E = \frac{1}{2}\rho \cdot W^3 \quad \text{where } \rho \text{ is the air density.} \tag{8}$$

A number of works have computed the wind power over ocean areas (e.g. Liu et al. 2008), however there has been no detailed estimation of wind power over the entire Mediterranean Sea. The SeaWind datasets enable such an estimation, which is shown in Fig. 9a for the mean wind power at a 10 m height. The largest region of high power densities is located in the Gulf of Lion (>550 W m^{-2}). Some areas of wind channelled by land (the Gibraltar Strait and the strait between Sardinia and Corsica) and the Aegean Sea take mean wind power above 350 W m^{-2}. Regarding the Atlantic region, high wind power is found in the northwest Spanish coast.

Persistence of meteorological variables is defined as the tendency for weather episodes to continue for a certain period of time. Persistence is a characteristic that helps to understand and quantify the wind dynamics and the derived marine dynamics for which wind is the main forcing (waves, storm surges), it is a conditioning factor for navigation issues, and it is one of the dominant factors affecting the wind energy production, since wind speed must be kept

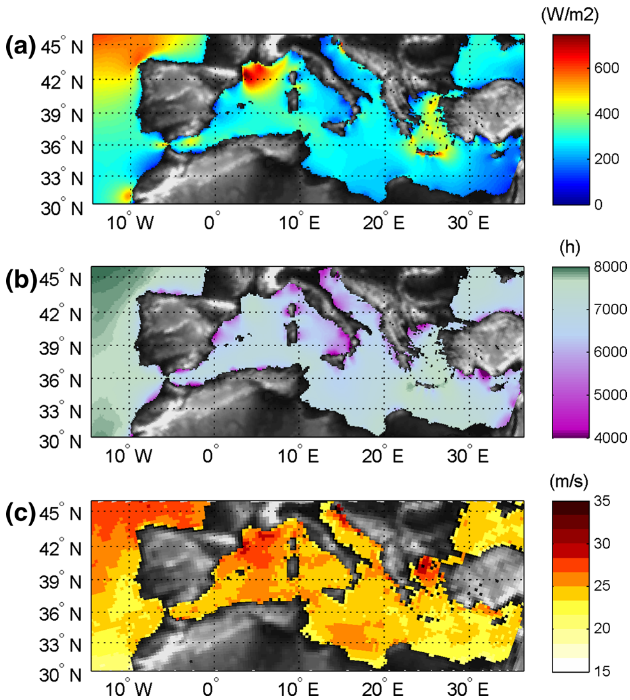

Fig. 9 Maps of (**a**) the wind power density at 10 m. From SeaWind II, in W/m2; (**b**) the ratio of hours per year between 2.5 and 25 m/s from SeaWind II; and (**c**) the 50-year return period wind speed (m/s) from SeaWind I

within an adequate interval for the sustainability of the wind energy resource. The number of hours per year that wind speed is between 2.5 and 25 m/s is a general indicator of the wind production. Figure 9b shows this duration for the analyzed spatial domain. Semi-enclosed areas with high orography near the coast have the lowest number of hours (i.e. Valencia gulf, Venice gulf, Southwest Tyrrhenian Sea and South Mediterranean coast of Turkey), while open sea areas in the Mediterranean (offshore Crete and northwestern Spain) have a larger duration.

Intense circulation systems with strong winds can have important social and economic impacts in the Mediterranean area contrasting with the usual pleasant weather. Long time series are needed for a proper estimation of extreme wind events. Therefore, the characterization of extreme winds has been assessed from the 60-year hourly SeaWind I dataset. The Generalized Extreme value (GEV) distribution is fitted to annual maxima at each grid point of the SeaWind I hindcast. The estimated 50-year return period wind speed is shown in Fig. 9c. Results indicate that the western Mediterranean basin has larger extreme winds than the Eastern basin and, aside from the Algerian coastline, the North shore presents stronger winds than the southern Mediterranean. The highest extreme wind speed occurs in the Gulf of Lion, eastern Adriatic Sea and northward Aegean Sea. In these regions, the estimated 50-year return period wind speed reached up to 30 m/s. Although the orographic flow-mountain perturbations and channelling effects contribute to gale winds, the primary cause of these extreme winds is a connection with cyclones located in or near the Mediterranean (Lionello et al. 2006a, b).

6 Summary and conclusions

A historical simulation of the surface offshore wind fields in southern Europe, covering the entire Mediterranean Sea, is presented. Two different products were developed using WRF as a tool to dynamically downscale global reanalysis data: SeaWind I (30-km horizontal resolution over a 60-year period) and SeaWind II (15-km horizontal resolution over a 20-year period).

The high-resolution hindcasts were obtained after a sensitivity test of the numerical model during a 3-month period in the western Mediterranean Sea. Different experimental setups were tested, including different PBL schemes, different running modes and different reanalyses as boundary forcings. The YSU PBL scheme provided only slightly better results than MYJ and ACM2. This is in agreement with recent results by García-Díez et al. (2012) for other surface variables over this area. A daily reforecast running mode represented wind variability and hour-to-hour correspondence better than simulations running freely in "climate" mode, using spectral nudging and, to a lesser extent, also better than the run using grid nudging. We assume that the results obtained for the selected region can be extended to the whole Mediterranean Sea because a wide variety of phenomena (complex topography, isolated islands, sea/land breeze, etc.) was included in the analysis of the sensitivity test. Concerning the global reanalysis used as boundary and initial conditions, the simulations using ERA-INTERIM showed more skill than those using ERA-40 or NCEP reanalysis. The latter showed the worst performance but, given that the differences were not large and that this reanalysis provides the longest period, the first product developed, SeaWind I, was based on NCEP reanalysis, as a previous work by Sotillo et al. (2005). A new-generation product, SeaWind II, was based on ERA-Interim at 15 km resolution.

A validation of the hindcast data was carried out in order to evaluate their reliability. The wind hindcasts were validated by comparing them with both, in situ hourly stations and wind altimeter observations from satellites. Several skill scores were estimated in order to evaluate the performance of the SeaWind downscalings. Results show overall a good agreement between instrumental measurements and wind hindcasts. The evaluation procedure confirms the suitability of the database and the WRF model to estimate historical sea surface wind situations. Therefore, this database can be the input to other applied studies such us surface ocean models.

This study has taken advantage of long duration datasets of sea winds with high resolution in space and time. A statistically robust characterization of climatologies and the probability distribution of surface wind were analyzed. The wind power, persistence of wind speed and the extreme wind speed events were also assessed. The geographical structure of these wind properties has been explained. Interesting local characteristics have been detected, such as areas of more than 350 W/m^2 of raw wind power at a height of 10 meters, coastal regions with <6000 hours of wind speed between 2.5 and 25 m/s, and the Mediterranean offshore regions with a 50 year return period wind speed higher than 25 m/s.

Acknowledgments The authors would like to thank Puertos del Estado (Spanish National Ports and Harbour Authority) for providing the information from the buoy records and model outputs from the HIPOCAS project. The work was partly funded by the projects iMar21 (CTM2010-15009) and CORWES (GL2010-22158-C02-01) from the Spanish government, and the FP7 European project CoCoNet (287844). The large amount of WRF simulations performed in this study were managed by WRF4G, which is an open-source tool funded by the Spanish government and co-funded by the European Regional Development Fund under grant CGL2011-28864.

References

Ardhuin F, Bertotti L, Bidlot J-R, Cavaleri L, Filipetto V, Lefevre J-M, Wittmann P (2007) Comparison of wind and wave measurements and models in the Western Mediterranean Sea. Ocean Eng 34:526–541

Arreola J, Homar V, Romero R, Ramis C, Alonso S (2003) Multiscale numerical study of the 10–12 November 2001 strong cyclogenesis event in the western mediterranean. In: MEDITERRANEAN STORMS-Proceedings of the 4th EGS Plinius conference, Mallorca, Spain, 2–4 October 2002, pp 1–4

Bauer E (1996) Characteristic frequency distributions of remotely sensed in situ and modelled wind speeds. Int J Climatol 16:1087–1102

Bengtsson L, Hagemann S, Hodges KI (2004) Can climate trends be calculated from reanalysis data? J Geophys Res 109:D11111

Brands S, Gutiérrez JM, Herrera S, Cofiño AS (2012) On the use of reanalysis data for downscaling. J Clim 25:2517–2526

Castro CL, Pielke SRA, Leoncini G (2005) Dynamical downscaling: assessment of value retained and added using the regional atmospheric modeling system (rams). J Geophys Res 110(D05):108

Cavaleri L, Bertotti L, Tescaro N (1996) Long term wind hindcast in the Adriatic Sea. Il Nuovo Cimento 19:67–89

Charney J, Halem M, Jastrow R (1969) Use of incomplete historical data to infer the present state of the atmosphere. J Atmos Sci 26:1160–1163

Chen F, Dudhia J (2001) Coupling an advanced land surface-hydrology model with the Penn State-NCAR MM5 modeling system. Part I. Model implementation and sensitivity. Mon Weather Rev 129:569–585

Chronis T, Papadopoulos V, Nikolopoulos EI (2011) QuickSCAT observations of extreme wind events over the Mediterranean and Black Seas during 2000–2008. Int J Climatol 31:2068–2077. doi:10.1002/joc.2213

Dee DP et al (2011) The ERA-Interim reanalysis: configuration and performance of the data assimilation system. Q J R Meteorol Soc 137:553–597

Dudhia J (1989) Numerical study of convection observed during the winter monsoon experiment using a mesoscale two-dimensional model. J Atmos Sci 46:3077–3107

Erickson DJ, Taylor JA (1989) Non-Weibull behavior observed in a model-generated global surface wind field frequency distribution. J Geophys Res 94(12):693–698

Fernández J, Montávez JP, Sáenz J, González-Rouco JF, Zorita E (2007) Sensitivity of MM5 mesoscale model to physical parameterizations for regional climate studies: annual cycle. J Geophys Res 112(D04):101

Feser F, Rockel B, von Storch H, Winterfeldt J, Zahn M (2011) Regional climate models add value. Bull Amer Meteor Soc 92:1181–1192

Fita L, Romero R, Ramis C (2007) Objective quantification of perturbations produced with a piecewise pv inversion technique. Ann Geophys 25:2335–2349

Fita L, Fernández J, García-Díez M (2010) Clwrf: Wrf modifications for regional climate simulation under future scenarios. In: Extended abstracts of the 11th WRF Users' Workshop, Boulder. 21–25 June 2010, pp 1–4

García-Díez M, Fernández J, Fita L, Yagüe C (2013) Seasonal dependence of WRF model biases and sensitivity to PBL schemes over Europe. Q J R Meteorol Soc 139:501–514

Genovés A, Jansà A (2003) Diabatic processes contribution to the november 2001 storm. In: MEDITERRANEAN STORMS-Proceedings of the 4th EGS Plinius conference, Mallorca. 2–4 October 2002, pp 1–4

Giorgi F (1990) Simulation of regional climate using limited area model nested in a general circulation model. J Clim 3:941–963

Grell G, Devenyi D (2002) A generalized approach to parameterizing convection combining ensemble and data assimilation techniques. Geophys Res Lett 29:1693. doi:10.1029/2002GL015311

Günter H, Rosenthal W, Stawarz M, Carretero JC, Gomez M, Lozano I, Serrano O, Reistad M (1997) The wave climate of the northeast Atlantic over the period 1955–1994: the was a wave hindcast. GKSS Forschungszentrum Geesthacht GmbH 73:1–34

Hong S, Lim J (2006) The WRF single-moment 6-class microphysics scheme (WSM6). J Korean Meteorol Soc 42:129–151

Hong S, Noh Y, Dudhia J (2006) A new vertical diffusion package with an explicit treatment of entrainment processes. Mon Weather Rev 134:2318–2341

Hsu SA, Meindl EA, Gilhousen DB (1994) Determining the power-law wind profile exponent under near-neutral stability conditions at sea. J Appl Meteorol 33(6):757–765

Hu X-M, Nielsen-Gammon JW, Zhang F (2010) Evaluation of three planetary boundary layer schemes in the WRF model. J Appl Meteor Climatol 49:1831–1844

Jacob D, Podzun R (1997) Sensitivity studies with the regional climate model REMO. Meteorol Atmos Phys 63:119–129

Janjić ZI (1990) The step-mountain coordinate: physical package. Mon Weather Rev 118:1429–1443

Janjić ZI (1994) The step-mountain eta coordinate model: further developments of the convection, viscous sublayer, and turbulence closure schemes. Mon Weather Rev 122:927–945

Janjić ZI (2002) Nonsingular implementation of the Mellor–Yamada level 2.5 scheme in the NCEP Meso model. NCEP Office Note No. 437

Jiménez PA, Dudhia J (2012) Improving the Representation of Resolved and Unresolved Topographic Effects on Surface Wind in the WRF Model. J Appl Meteorol Climatol 51(2):300–316

Kalnay E, Kanamitsu M, Kistler R, Collins W, Deaven D, Gandin L, Iredell M, Saha S, White G, Woollen J, Zhu Y, Leetmaa A, Reynolds R, Chelliah M, Ebisuzaki W, Higgins W, Janowiak J, Mo KC, Ropelewski C, Wang J, Jenne R, Joseph D (1996) The ncep/ncar 40-year reanalysis project. B Am Meteorol Soc 77:437–471

Lenderink G, van Meijgaard E, Selten F (2009) Intense coastal rainfall in the netherlands in response to high sea surface temperatures: analysis of the event of August 2006 from the perspective of a changing climate. Clim Dyn 32(1):19–33

Lionello P, Malanotte-Rizzoli P, Boscolo R (eds) (2006a) Mediterranean climate variability. Elsevier, Amsterdam

Lionello P, Bhend J, Buzzi A, Della-Marta PM, Krichak SO et al (2006b) Cyclones in the Mediterranean region: climatology and effects on the environment. Dev Earth Environ Sci 4:5463–5467

Liu WT, Tang W, Xie X (2008) Wind power distribution over the ocean. Geophys Res Lett 35(L13808):6

Lo J, Yang Z, Pielke R Sr (2008) Assessment of three dynamical climate downscaling methods using the weather research and forecasting (wrf) model. J Geophys Res 113(D09):112

Marcos M, Tsimplis MN, Shaw AGP (2009) Sea level extremes in southern Europe. J Geophys Res 114:C01007. doi:10.1029/2008JC004912

Mlawer E, Taubman S, Brown P, Iacono M, Clough S (1997) Radiative transfer for inhomogeneous atmospheres: RRTM, a validated correlated-k model for the long wave. J Geophys Res 102(D14):16663–16682

Monahan AH (2006) The probability distribution of sea surface wind speeds. Part I: theory and SeaWinds observations. J Clim 19(4):497–520

Pavia EG, O'Brien JJ (1986) Weibull statistics of wind speed over the ocean. J Clim Appl Meteorol 25:1324–1332

Pleim JE (2006) A simple, efficient solution of flux–profile relationships in the atmospheric surface layer. J Appl Meteorol Climatol 45:341–347

Pleim JE (2007a) A combined local and nonlocal closure model for the atmospheric boundary layer. Part I: Model description and testing. J Appl Meteorol Climatol 46:1383–1395

Pleim JE (2007b) A combined local and nonlocal closure model for the atmospheric boundary layer. Part II: Application and evaluation in a mesoscale meteorological model. J Appl Meteorol Climatol 46:1396–1409

Pryor SC, Nielsen M, Barthelmie RJ, Mann J (2004) Can satellite sampling of offshore wind speeds realistically represent wind speed distributions? Part II: quantifying uncertainties associated with distribution fitting methods. J Appl Meteorol 43:739–750

Qian J, Seth A, Zebiak S (2003) Reinitialized versus continuous simulations for regional climate downscaling. Mon Weather Rev 131(11):2857–2874

Rockel B, Castro CL, Pielke RSA, von Storch H, Leoncini G (2008) Dynamical downscaling: assessment of model system dependent retained and added variability for two different regional climate models. J Geophys Res 113(D21):107

Sanchez-Vidal A, Canals M, Calafat AM, Lastras G, Pedrosa-Pa'mies R et al (2012) Impacts on the deep-sea ecosystem by a severe coastal storm. PLoSONE 7(1):e30395. doi:10.1371/journal.pone.0030395

Skamarock WC, Klemp JB, Dudhia J, Gill DO, Baker DM, Duda MG, Huang XY, Wang W, Powers JG (2008). A description of the advanced research WRF version 3. NCAR Tech Note NCAR/TN-475 + STR, p 125

Sotillo MG, Ratsimandresy AW, Carretero JC, Bentamy A, Valero F, González-Rouco F (2005) A high-resolution 44-year atmospheric hindcast for the mediterranean basin: contribution to the regional improvement of global reanalysis. Clim Dyn 25:219–236

Stauffer DR, Seaman NL (1990) Use of four-dimensional data assimilation in a limited-area mesoscale model. Part I: experiments with synoptic-scale data. Mon Weather Rev 118:1250–1277

Taylor KE (2001) Summarizing multiple aspects of model performance in a single diagram. J Geophys Res 106:7183–7192

Uppala S, Kallberg P, Simmons A, Andrae U, da Costa Bechtold V, Fiorino M, Gibson J, Haseler J, Hernandez A, Kelly G, Li X, Onogi K, Saarinen S (2005) The era-40 re-analysis. Q J R Meteorol Soc 131:2961–3012

Von Storch H, Langenberg H, Feser F (2000) A spectral nudging technique for dynamical downscaling purposes. MWR 128:3664–3673

WASA group (1998) Changing waves and storms in the northeast atlantic? BAMS 79(5):741–760

Weisse R, Feser F (2003) Evaluation of a method to reduce uncertainty in wind hindcasts performed with regional atmosphere models. Coast Eng 48:211–225

Weisse R, von Storch H, Callies U, Chrastansky A, Feser F, Grabemann I, Günther H, Pluess A, Stoye T, Tellkamp J, Winterfeldt J, Woth K (2009) Regional meteorological-marine reanalyses and climate change projections: results for Northern Europe and potential for coastal and offshore applications Bull. Am Meteorol Soc 90(6):849–860

Weisse R, von Storch H, Niemeyer HD, Knaack H (2012) Changing North Sea storm surge climate: An increasing hazard? Ocean Coast Manag 68:58–68

Winterfeldt J, Weisse R (2009) Assessment of value added for surface marine wind speed obtained from two regional climate models. Mon Weather Rev 137(9):2955–2965

Winterfeldt J, Geyer B, Weisse R (2011) Using QuikSCAT in the added value assessment of dynamically downscaled wind speed. Int J Climatol 31:1028–1039